Microscopic Insight into Temperature-Graded Ferroelectrics

Qingteng Zhang and I. Ponomareva*

Department of Physics, University of South Florida, Tampa, Florida 33620, USA

(Received 8 June 2010; published 28 September 2010)

A microscopic approach based on the first-principles effective Hamiltonian is developed to study the polarization response in temperature-graded ferroelectrics. This approach has been applied to the case of $(Ba_{0.75}Sr_{0.25})TiO_3$ alloy. A comparison of the computational results with available experimental data attests to the remarkable accuracy of the present approach. Our computations reveal a strong anisotropy in the response of polarization to the temperature gradient (TG). In particular, the polarization offset along the direction of TG is an order of magnitude lower than in the perpendicular direction. The large as well as the small TGs are considered and found to yield qualitatively different polarization field responses. Among other striking findings are (i) the coexistence of different phases in chemically homogeneous regions, (ii) formation of low-symmetry phases, and (iii) thermally controlled polarization rotation.

DOI: 10.1103/PhysRevLett.105.147602 PACS numbers: 77.22.Ej, 77.80.Fm

Graded ferroelectrics have attracted a lot of attention in recent years, owing to their many remarkable properties [1–6], and in light of the elevated interest in thermoelectric materials. The term graded ferroelectric usually refers to a ferroelectric exhibiting polarization gradient. These polarization gradients can be caused by composition, stress, or temperature gradients (TGs) and result in dramatic hysteresis loop offsets, transpacitor behavior, enormous pyroelectric responses, and other exotic properties [1–6]. It was shown experimentally that both ''up'' and ''down'' hysteresis offsets can be achieved by introducing TG in $(Ba_{0.75}Sr_{0.25})TiO_3$ ceramics [1]. In this ground-breaking experiment a TG was established along the polarization direction and yielded highly nonlinear polarization offsets for temperatures near the Curie point (T_C). A phenomenological approach was subsequently developed to reproduce experimental observations [2]. These works have demonstrated the potential advantages of temperature-graded ferroelectrics that include (1) reversibility of polarization gradient and built-in potential, (2) the possibility of controlling the gradient magnitude and, therefore, the built-in potential, and (3) the ability to thermally tune the responses of ferroelectrics. Interestingly, despite all these exciting developments, our understanding of polarization-graded ferroelectrics is still limited. For example, the origin of hysteresis offsets is still very much controversial. Several models have been proposed to explain such offsets, including the existence of a built-in potential associated with the polarization gradient [1–3,5,7], formation of polydomain state [8,9], and artifacts associated with free charge or asymmetric leakage current [4].

The aims of this Letter are (1) to gain a fundamental microscopic understanding of the temperature-graded ferroelectrics through the development and use of an accurate first-principles-based computational approach, (2) to reveal the unexpected phenomena associated with the temperature grading, and (3) to demonstrate the unusual effects that nonequilibrium conditions can have on the material properties.

Specifically, in this Letter, we develop a computational approach that allows accurate atomistic simulations of the effect of TG on the properties of perovskite ferroelectrics. Our decision to focus on the ferroelectric alloy $(Ba_{0.75}Sr_{0.25})TiO_3$ is based on the availability of some experimental data for this alloy [1]. The alloy is modeled by $12 \times 12 \times 31$ supercell (22 320 atoms), which is periodic along all three directions to simulate the bulk system. We chose x, y, and z axes to lie along the (100), (010), and (001) crystallographic directions, respectively. The total energy of this supercell is given by the first-principles-based effective Hamiltonian [10] that depends on the local soft mode (which is proportional to the electric dipole moment), inhomogeneous and homogeneous strain variables, and alloy configuration. It includes a local mode self-energy (harmonic and unharmonic contributions), a long-range dipole-dipole interaction, a short-range interaction between local modes, an elastic energy, the interaction between the local modes and strains, and the interactions responsible for alloying effects. This Hamiltonian correctly reproduces the complex sequence of phase transitions in $(Ba_xSr_{1-x})TiO_3$ alloys for a wide compositional range [11] and yields results in good agreement with both experiment and first-principles calculations (see Refs. [10,12,13]).

To simulate the TG we use the direct method that is analogous to the experimental method. This method requires the use of nonequilibrium molecular dynamics (MD) that has been previously utilized to simulate transport properties, such as thermal conductivity or diffusion. The supercell used in the calculation is divided into $N = 31$ slabs along the direction of the measurement (z axis in our case). One of these slabs is used as a heat source, while another is used as a heat sink [14]. For every MD step each particle velocity in the source (sink) region is

scaled by the same factor so that the resulting kinetic energy is increased (decreased) by an amount $\Delta\epsilon$ and a heat flux $\Delta\epsilon/\Delta t$ is generated along the z direction. Here Δt is the duration of a single MD time step. The system is then allowed to reach steady state with the resultant TG controlled by the magnitude of the heat flux. We begin our simulations by equilibrating the system at the desired temperature T^{eq} using 500 000 MD steps within the NVT ensemble. The heat flux is then turned on and the simulations are continued for another 4 000 000 MD steps. The last 1 000 000 MD steps are used for computing averaged values of polarization, temperature, and other properties [15]. We consider two possible mechanical boundary conditions: (i) the unclamped (or stress-free) sample and (ii) the clamped (or strained) sample. Computationally, the unclamped sample is simulated by allowing all components of the homogeneous strain tensor [16] to relax, while clamping is achieved by freezing out the strain [17]. To achieve a realistic clamping we fix the homogeneous strain at its equilibrium value for a given temperature T^{eq}.

We begin by considering the clamped sample since it is believed that the electrodes in the experimental setup for measurements on temperature-graded ferroelectrics may provide this clamping [2]. We first check the accuracy of our simulations by comparing computational data obtained for the $(Ba_{0.75}Sr_{0.25})TiO_3$ alloy near T_C with the available experimental data [1]. The results of our simulations for a sample in the tetragonal state with polarization along the z direction are given in Fig. 1. The top panel shows the temperature profile along the z axis, while the bottom panel shows the change in polarization $\Delta P_z(z) = P_z^{\mathrm{noneq}}(z) - P_z^{\mathrm{eq}}(z)$ associated with this temperature profile. Here $P_z^{\mathrm{noneq}}(z)$ is the polarization in the sample that is subject to the TG (nonequilibrium conditions), while P_z^{eq} is the polarization in the same sample when no TG exists (equilibrium conditions). The average temperature of the sample is 310 K. To eliminate contributions of the heat source and sink, we focus on the region between the 4th and the 13th slabs of the supercell (the region shown between the two vertical lines in Fig. 1). We will refer to the leftmost (rightmost) boundary of this region as the hot (cold) slab. In between the hot and cold slabs the temperature varies linearly along the sample giving rise to a TG of -7.3 K/nm. The difference in temperature between the cold and hot slabs is $\Delta T = T^{\mathrm{cold}} - T^{\mathrm{hot}} = -26$ K. The linear difference in the temperature gives rise to a corresponding linear variation of polarization (see bottom panel of Fig. 1). The sample remains in the tetragonal state. We can now calculate the polarization offset between the cold and the hot slabs as [18] $\Delta P_z^{\mathrm{offset}} = P_z^{\mathrm{noneq}}(z_{\mathrm{cold}}) - P_z^{\mathrm{noneq}}(z_{\mathrm{hot}}) = \Delta P_z(z_{\mathrm{cold}}) - \Delta P_z(z_{\mathrm{hot}})$, which gives $\Delta P_z^{\mathrm{offset}} = 0.033\ \mu\mathrm{C/cm}^2$ for $\Delta T = -26$ K, in excellent agreement with experimental findings of Ref. [1] that reported $0.030 \pm 0.004\ \mu\mathrm{C/cm}^2$ for the same $T^{\mathrm{cold}} = 300$ K and ΔT. The existence of polarization gradient results in the built-in, or internal, electric field $E_z^{\mathrm{int}}(z) = -[z/\epsilon_0\epsilon_r(z)]dP_z/dz$ [2], which in our case of the linear

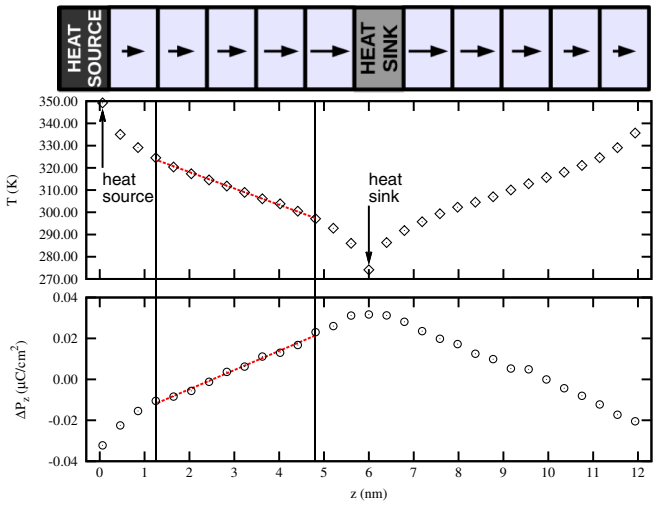

FIG. 1 (color online). The temperature (top panel) and polarization (bottom panel) profiles along the simulation supercell achieved by using $\Delta\varepsilon/\Delta t = 3.2$ meV/fs near $T^{\mathrm{eq}} = 310$ K. The symbols correspond to the computational data, while the dashed lines give a linear fit. The schematization of the simulation supercell is given at the top of the figure.

polarization profile gives an average built-in field of -0.39 kV/cm in the region between the cold and hot slabs of the sample. Furthermore, we find that the polarization offset disappears for $\Delta T = 40$ K, in agreement with experimental findings of Ref. [1]. Our atomistic simulations indicate that under these conditions the average temperature of the sample is 320 K (5 K above the Curie temperature) and $\Delta P_z(z) = 0$ in between the cold and the hot slabs, which explains the disappearance of polarization offset. We therefore conclude that our computations accurately reproduce experimental observations. A more detailed comparison, however, is not possible due to the structural and dimensional differences between the samples used in computations and experiments.

It is worth noting that the case that we just described, as well as the works of Refs. [1,2], assumes that ΔT is computed with respect to the $T(z_{\mathrm{cold}})$, while the latter is kept fixed. We will now take advantage of our computational technique to study a different scenario, where the temperatures of the hot (cold) slab is given by $T(z_{\mathrm{hot}}) = T^{\mathrm{eq}} + \Delta T/2$ [$T(z_{\mathrm{cold}}) = T^{\mathrm{eq}} - \Delta T/2$]. In other words, we will study the gradients that are symmetric with respect to T^{eq} and denoted as $\frac{dT}{dz}|_{T=T^{\mathrm{eq}}}$. We begin by considering the case $T^{\mathrm{eq}} = 280$ K. Under equilibrium conditions the sample assumes a ferroelectric tetragonal state with polarization along the z axis. We next apply different ΔT and observe the polarization offset associated with it. Our results are shown in Fig. 2 and reveal many striking features. First, we notice that the polarization offset along the z direction is a linear function of ΔT for all gradients considered. Another interesting feature is the existence of two regions that are described by a different slope κ_{zz} as defined from $\Delta P_\alpha^{\mathrm{offset}}/\Delta x_\beta = \kappa_{\alpha\beta}(\Delta T/\Delta x_\beta)$, where α and β correspond to Cartesian coordinates. The first one

($\kappa_{zz} = -2.1$ nC/cm^2 K) corresponds to the case of relatively small ΔT (see solid line in Fig. 2), while the second one ($\kappa_{zz} = -1.4$ nC/cm^2 K) is associated with an extremely large ΔT. We now take advantage of our microscopic simulations to understand the origin of the double-slope behavior. It turns out that the change in the slope as we increase ΔT is associated with formation of monoclinic phase. Since in the limit of large ΔT the temperature of the cold slab is below the tetragonal to orthorhombic transition temperature, this leads to a ''mixing'' of orthorhombic and tetragonal phases which, in turn, results in the formation of monoclinic phase. This monoclinic phase originates near the cold slab and may extend far in the sample resulting in continuous polarization rotation across the sample. Moreover, the ability to induce a monoclinic phase by introducing temperature inhomogeneity, such as the TG, may have an important technological implication, since these low-symmetry phases that result from polarization rotation are known to yield high dielectric and piezoelectric responses. In addition, such responses can be tuned thermally. It should be noted, however, that while our computational technique is very accurate for the limits of both large and small ΔT, it may be less accurate in the intermediate region due to the periodicity of the computational supercell. Therefore, the region where the transition from tetragonal to monoclinic phase occurs should be considered qualitatively, rather than quantitatively. We observed the double-slope behavior for all temperatures considered. The third interesting feature of Fig. 2 is an extremely large value of $\Delta P_z^{\text{offset}}$ that can be obtained by applying TGs.

Next we investigate the temperature dependence for the slope κ_{zz} that describes the polarization offset in the limit of small ΔT. If we assume that in each slab the polarization simply follows the usual dependence $P^{\text{eq}}(T)$ associated with the equilibrium conditions, then we can expect that the largest magnitude for κ_{zz} would occur at the temperature for which the derivative $\partial P^{\text{eq}}(T)/\partial T$ is at an extremum, i.e., around T_C. Contrary to our expectations the extremum of κ_{zz} occurs at 280 K, which is 35 K below T_C (see inset of Fig. 2). The reason for this behavior is the enormous resistance of the sample to the polarization gradients, which results in the linear dependence of the polarization on the temperature along the direction of temperature (and polarization) gradient. This is true even for the temperature region where $P^{\text{eq}}(T)$ is a nonlinear function. As a result, the slope κ_{zz} is minimized not at the temperature at which the derivative $\partial P^{\text{eq}}(T)/\partial T$ is at extremum but rather at the temperature where $\partial P^{\text{eq}}(T)/\partial T$ is a constant. In other words, we observe the minimum of κ_{zz} to occur at the temperature near which P^{eq} is a linear function of T since it provides the most natural environment for linear polarization gradients. On the other hand, near the Curie point P^{eq} is a nonlinear function of T, and, therefore, in conflict with the linear behavior dictated by the temperature (and polarization) gradient.

So far we have reported data obtained for the case where the polarization vector lies along the direction of TG (longitudinal case). The case of the polarization vector perpendicular to the TG direction (transverse case, see Fig. 3) is described next. First, we notice that for the case when T_{cold} is held fixed at ≈ 300 K the polarization offset disappears around $\Delta T = 20$ K, which is quite different from the longitudinal case. To make a further comparison between the transverse and the longitudinal case, we plot $\Delta P_y^{\text{offset}}$ as a function of ΔT at $T^{\text{eq}} = 280$ K (see Fig. 3). Immediately we see that the polarization offset is an order of magnitude higher as compared to the longitudinal case. In other words, the transverse component of polarization is more responsive to TG than the longitudinal one. This can be explained from the electrostatic point of view by

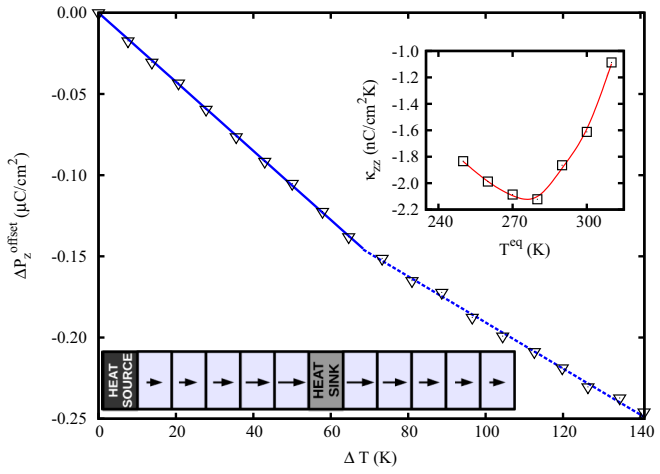

FIG. 2 (color online). The polarization offset ($\Delta P_z^{\text{offset}}$) between cold and hot slabs as a function of the temperature difference ΔT computed at $T^{\text{eq}} = 280$ K. The inset shows the dependence of the slope κ_{zz} on the temperature T^{eq} in the limit of small ΔT. The line is a guide for the eye. The schematization shows the polarization direction for the longitudinal case.

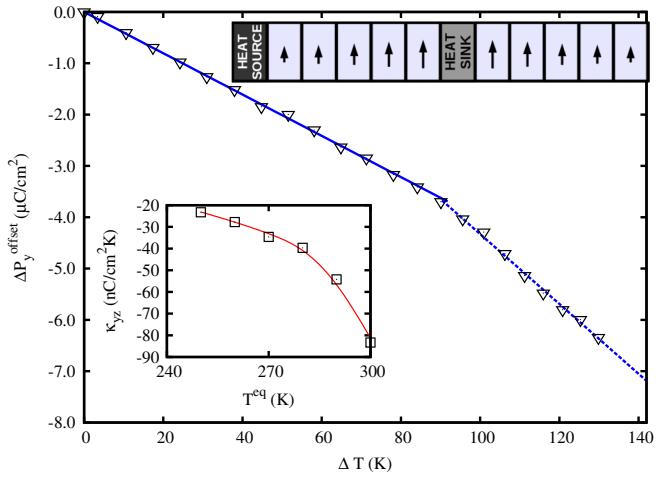

FIG. 3 (color online). The polarization offset ($\Delta P_y^{\text{offset}}$) between cold and hot slabs as a function of the temperature difference ΔT computed at $T^{\text{eq}} = 280$ K. The inset shows the dependence of the slope κ_{yz} on the temperature T^{eq} in the limit of small ΔT. The line is a guide for the eye. The schematization shows the polarization direction for the transverse case.

considering the interaction between the local dipoles. We can relate the case of transverse and longitudinal polarization gradient to the case of transverse and longitudinal optical modes. The local fields acting on the local dipole moments are different in these two cases, which leads to the softening of the transverse optical mode and stiffening of the longitudinal optical mode. In the presence of TGs the same local fields can lead to a stronger resistance to polarization gradient in the longitudinal case and much weaker resistance to polarization gradient in the transverse case. To further strengthen this conclusion we plot the slope κ_{yz} as a function of the temperature T^{eq} for the transverse case and small ΔT (see inset of Fig. 3). Contrary to the longitudinal case, we now observe that the slope κ_{yz} reaches its largest magnitude around T_C, as expected from the $P^{\mathrm{eq}}(T)$ dependence. Figure 3 also reveals that κ_{yz} exhibits a double-slope behavior. However, qualitatively such double-slope behavior is different from the longitudinal case since the second slope is actually steeper than the first one. Interestingly, the onset of the second slope appears to be due to the formation of a paraelectric region near the hot slab of the sample.

Next we are interested in seeing how our results will change for the case of the unclamped sample. In the limit of small TGs, the data are very similar to that for the clamped sample since such small perturbations preserve the sample averages for polarization, temperature, and strain. In other words, under such conditions the average polarization, temperature, and most importantly, strain are very close to their equilibrium values and therefore the sample response to the TG is nearly identical for the clamped and unclamped cases. The most striking discovery is the longitudinal polarization behavior under large TGs. Our simulations reveal that for large TGs the polarization rotates from the longitudinal to the transverse direction. In other words, applying a large TG along the direction of polarization under stress-free conditions will cause the polarization to rotate by 90°. This is again consistent with our findings that the sample has much higher resistance to polarization gradients along the polarization direction when compared to the polarization gradients along the perpendicular direction. In our simulations keeping the cold slab at 216 K and the hot slab at 328 K led to a 90° polarization rotation that completed within 4 ns.

In summary, we have proposed a computational approach that allows atomistic study of ferroelectric materials under nonequilibrium conditions, such as TGs. Application of this approach to study the influence of TGs on the polarization fields in $(Ba_{0.75}Sr_{0.25})TiO_3$ alloys revealed that TGs lead to reversible and controllable polarization offsets, built-in electric fields, and even polarization rotation. These findings could lead to important technological advancements, since built-in electric fields can be utilized in various applications including transpacitors with a giant energy gain [19], energy converters (to convert ubiquitous TGs into electrical signals), thermally tunable devices (where the piezoelectric and dielectric responses are controlled by the TG), photovoltaics (where the built-in electric fields are used to separate the carriers and reduce the recombination rate), and others. The possibility of being able to control the polarization direction by introducing local temperature inhomogeneity may lead to unusual thermally controlled devices including ferroelectric memories. We have also provided a microscopic explanation for our findings and believe that most of our conclusions are general and valid for a whole class of polarization-graded ferroelectrics, regardless of how the polarization gradient is achieved.

The authors would like to acknowledge the use of the services provided by Research Computing, University of South Florida. I. P. acknowledges support from the University of South Florida under Grant No. R070699.

*iponomar@usf.edu

[1] W. Fellberg *et al.*, Appl. Phys. Lett. **78**, 524 (2001).
[2] S. P. Alpay, Z.-G. Ban, and J. V. Mantese, Appl. Phys. Lett. **82**, 1269 (2003).
[3] S. Zhong *et al.*, Appl. Phys. Lett. **89**, 142913 (2006).
[4] H. K. Chan, C. H. Lam, and F. G. Shin, J. Appl. Phys. **95**, 2665 (2004).
[5] L. Pintilie, I. Boerasu, and M. J. M. Gomes, J. Appl. Phys. **93**, 9961 (2003).
[6] M. B. Okatan, J. V. Mantese, and S. P. Alpay, Phys. Rev. B **79**, 174113 (2009).
[7] S. Zhong, S. P. Alpay, and J. V. Mantese, Appl. Phys. Lett. **87**, 102902 (2005).
[8] A. A. Bogomolov and A. V. Solnyshkin, Crystallogr. Rep. **50**, S53 (2005).
[9] A. L. Roytburd and J. Slutsker, Appl. Phys. Lett. **89**, 042907 (2006).
[10] L. Walizer, S. Lisenkov, and L. Bellaiche, Phys. Rev. B **73**, 144105 (2006).
[11] In case of $(Ba_{0.75}Sr_{0.25})TiO_3$ solid solution the effective Hamiltonian predicts transition from a cubic paraelectric phase to a tetragonal ferroelectric phase at 315 ± 5 K (320 K), from a tetragonal to an orthorhombic phase at 235 ± 5 K (235 K), and from an orthorhombic to a rhombohedral phase at 185 ± 5 K (165 K) [10]. The data in brackets indicate the experimental value for the same transition.
[12] I. Ponomareva *et al.*, Phys. Rev. B **77**, 012102 (2008).
[13] J. Hlinka *et al.*, Phys. Rev. Lett. **101**, 167402 (2008).
[14] P. Jund and R. Jullien, Phys. Rev. B **59**, 13 707 (1999).
[15] This computational setup is designed to accurately compute polarization response to a given TG. It does not predict how (or whether) such TGs can be achieved.
[16] W. Zhong, D. Vanderbilt, and K. M. Rabe, Phys. Rev. B **52**, 6301 (1995).
[17] Note that inhomogeneous, or local, strains are fully relaxed for both clamped and unclamped cases.
[18] Note that the expression for $\Delta P_z^{\mathrm{offset}}$ implies that $P_z^{\mathrm{eq}}(z_{\mathrm{cold}}) = P_z^{\mathrm{eq}}(z_{\mathrm{hot}})$. This allows us to isolate the temperature induced contribution to the polarization gradient.
[19] J. V. Mantese, N. W. Schubring, and A. L. Micheli, Appl. Phys. Lett. **79**, 4007 (2001).